

Milky Way Gas Dynamics¹

Peter Englmaier
Peter.Englmaier@unibas.ch
+41-61-2055-434

Departement für Physik und Astronomie,
Astronomisches Institut, Universität Basel,
Venusstr. 7, 4102 Binningen, Switzerland

Ortwin Gerhard
gerhard@mpe.mpg.de
+41-61-30000-3539

Max-Planck-Institut für Extraterrestrische Physik,
Giessenbachstrasse, 85748 Garching bei München, Germany

October 31, 2018

¹Invited talk at the AAS Division on Dynamical Astronomy meeting, Santa Barbara, April 2005

Abstract

The Milky Way is made up of a central bar, a disk with embedded spiral arms, and a dark matter halo. Observational and theoretical constraints for the characteristic parameters of these components will be presented, with emphasis on the constraints from the dynamics of the Milky Way gas. In particular, the fraction of dark matter inside the solar radius, the location of the main resonances, and the evidence for multiple pattern speeds will be discussed.

1 Introduction

In our current understanding of the universe galaxies evolve within dark matter halos during the expansion of the universe. Very successfully, the theory of hierarchical clustering and merging of dark matter halos explains the structure on large scales and the variety of galaxy masses and types observed. Yet, on smaller scales the details of dissipation, star formation, and secular evolution, which also depend on non-gravitational forces, become more important and need to be addressed. Observations and detailed modeling is required to help understand the processes of galactic evolution.

Our own galaxy is particularly important in this respect, because it allows much more detailed observations, down to stellar proper motions around the central black hole and planet formation around young stars. Many new large surveys of the visible matter inventory of the Milky Way are under way: the survey RAVE hopes to measure radial velocities and chemical abundances of the brightest 50 million stars, the space interferometry mission SIM will accurately determine the distance to the galactic center and the local standard of rest (LSR) velocity, and GLIMPSE, a Spitzer Legacy Science Program, already built a catalog of 47 million sources in the longitude range $10^\circ \leq |l| \leq 64^\circ$ within the galactic plane $|b| \leq 1^\circ$, to be extended to fill the gap within $|l| \leq 10^\circ$. The goal of these surveys is to understand the Milky Way's present state and formation history (Benjamin *et al.* 2005; Majewski *et al.* 2004; Steinmetz 2003).

Detailed modeling of the Milky Way is required to make sense of these data sets. Because of our position within the galactic plane, we cannot grasp the large-scale structure easily. With certain symmetry assumptions, however, it is possible to recover the present 3-dimensional structure. In the following, we review the steps necessary for deriving such a model.

2 Luminosity model

Traditionally, mass models for the Milky Way have been constructed from parametrized analytical descriptions of the individual components: bulge, thin and thick disk, bar, and halo. The most successful axisymmetric model was published by Kent (1992) who used IRAF data to describe the stellar matter distribution. Later Dwek *et al.* (1995) used the COBE/DIRBE near-infrared maps of the inner Galaxy to fit a tri-axial bulge and double-exponential disk to the near-IR data. This approach was so successful — for the first time the bar of the Milky Way was directly seen — that a

number of more detailed studies were triggered. However, any division into components is to some degree arbitrary, and parametric models have serious limitations.

Another route was taken by Fux (1997), who generated a large number of bar forming n-body models. By selecting the model closest to the observed COBE/DIRBE light distribution he was able to reproduce the observations. The method is limited by the number of models one can generate; and there is no guarantee that and how well the Milky Way fits in the space spanned by the n-body models evolved from the chosen initial conditions.

A more generic approach was adopted by Binney and Gerhard (1996) and Bissantz and Gerhard (2002), who developed and applied new non-parametric methods, to fit the observed near-IR light distribution as measured by COBE/DIRBE. Both methods require the specification of an initial model which is subsequently adjusted to simultaneously minimize the deviations from the observations, smoothness and penalty term. With some reasonable symmetry assumptions, these methods yield the approximate 3-dimensional light distribution of the inner Galaxy on a model grid which can then be analyzed to extract parametric information, such as disk scale length or bar axis ratio and radial extent.

When adding a gaseous component, the bar in this model can drive spiral arms similar to the observed spiral pattern. However, a more realistic treatment of the spiral arms was introduced by Bissantz and Gerhard (2002) who allowed for deviations from triaxial symmetry, and added an analytical spiral arm model known to fit the observed spiral arm pattern rather well, and took it into account when inverting the light distribution. Interestingly, a model with spiral arm contribution to the COBE/DIRBE light makes the deduced bar longer and more elongated compared to models without spiral arms. Furthermore, only a model with spiral arm contribution can produce the observed asymmetries in the red clump line-of-sight distributions (Bissantz and Gerhard 2002). This result demonstrates how important it will be to combine different data sets from different observations.

The modeling results depend to some extent on the assumed solar galactocentric radius R_{\odot} and local standard of rest (LSR) velocity V_{\odot} . Reid (1993) reviewed measurements of R_{\odot} and found 8 ± 0.5 kpc, while more recently Eisenhauer *et al.* (2003) estimated the distance to the galactic center black hole to be 7.94 ± 0.42 kpc, still with a relative error of 5%. The LSR velocity is then inferred from Hipparcos data, coming out to be 218 ± 21 km s⁻¹ (Feast and Whitelook 1997). Most of the uncertainty comes from the R_{\odot} error. A new analysis, taking into account previously ignored systematic effects, was published by Kalirai *et al.* (2004) showing that the LSR velocity

might be lower, only $203 \pm 25 \text{ km s}^{-1}$. Reid and Brunthaler (2004) on the other hand found a higher value from the proper motion of Sgr A*: $V_{\odot} = 236 \pm 15 \text{ km s}^{-1}$. Here we assume a solar galactocentric radius $R_{\odot} = 8 \text{ kpc}$ and a LSR velocity $V_{\odot} = 220 \text{ km s}^{-1}$.

3 Mass model

Assuming a spatially constant mass-to-light ratio, the NIR luminosity model can be converted to a mass model. In reality, the mass-to-light ratio of a stellar population depends on age and metallicity of the underlying stellar population, which would vary within the Milky Way, but these dependencies are weaker than in the optical. The luminous Galaxy is probably embedded in a dark matter halo, which makes the circular rotation curve flat in the outer parts. Combining the luminosity model and the constant M/L assumption for the stars with an analytical model for the dark matter distribution, a mass model can be constructed with only a few free parameters: the mass-to-light ratio for the visible component(s), the position angle of the bar, the pattern speeds of bar and spiral pattern, and the halo model parameters.

For the invisible dark matter halo, we assume a logarithmic density profile with two parameters: scale radius a and velocity V . We find below that the details of the assumed profile do not matter, as long as the rotation curve of the dark halo is proportional to radius within the region probed by the data, i.e. inside R_{\odot} . Therefore, the dark matter halo model truly has only one free parameter, the slope at small radii V/a , where a can be anything larger than 10 kpc .

The combined total rotation curve can be compared to the observed terminal velocity curve of the gas. When we assume that the luminous matter in the Milky Way has the maximal M/L allowed by the terminal curve, and a dark matter halo scale radius of $a = 10.7 \text{ kpc}$, the best fit is obtained with $V = 235 \text{ km s}^{-1}$. The result can be seen in Fig. 1. The deviation for $r < 2.5 \text{ kpc}$ is due to the bar which forces the gas on non-circular orbits. At larger radii, the agreement is very good, and apart from two small humps at 4 kpc and 6 kpc , the model fits as well as the scatter in the data allows. When the orbital motion of the Sun is added to the model's terminal velocity curve, we obtain the rotation curve in Fig. 2. One sees that the contribution of dark matter inside R_{\odot} in the model is less than the contribution of visible matter.

From Fig 1 we see that a surprisingly good fit to the data is obtained

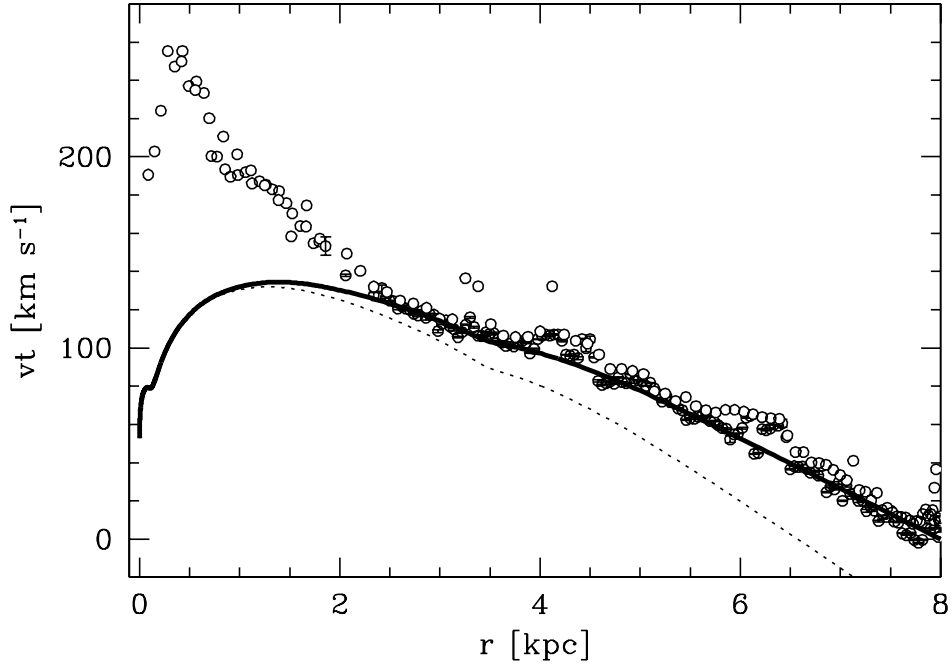


Figure 1: Comparison of model (solid curve) to a collection of terminal velocity curve data (symbols: ^{12}CO data from Clemens (1985), and HI data from Burton and Liszt (1993); Fich *et al.* (1989)). The lower dotted curve corresponds to the visible light contribution. For this fit, we assume $R_{\odot} = 8 \text{ kpc}$ and solve for the LSR velocity. The fit is required to match zero terminal velocity at R_{\odot} and the only free parameters varied are the halo velocity scale V and the mass-to-light ratio for the visible matter, which depends weakly on the assumed V . By adjusting V we were able to match the observed terminal velocity curve; the LSR velocity for this fit is $V_{\odot} = 221 \text{ km s}^{-1}$, in agreement with observations.

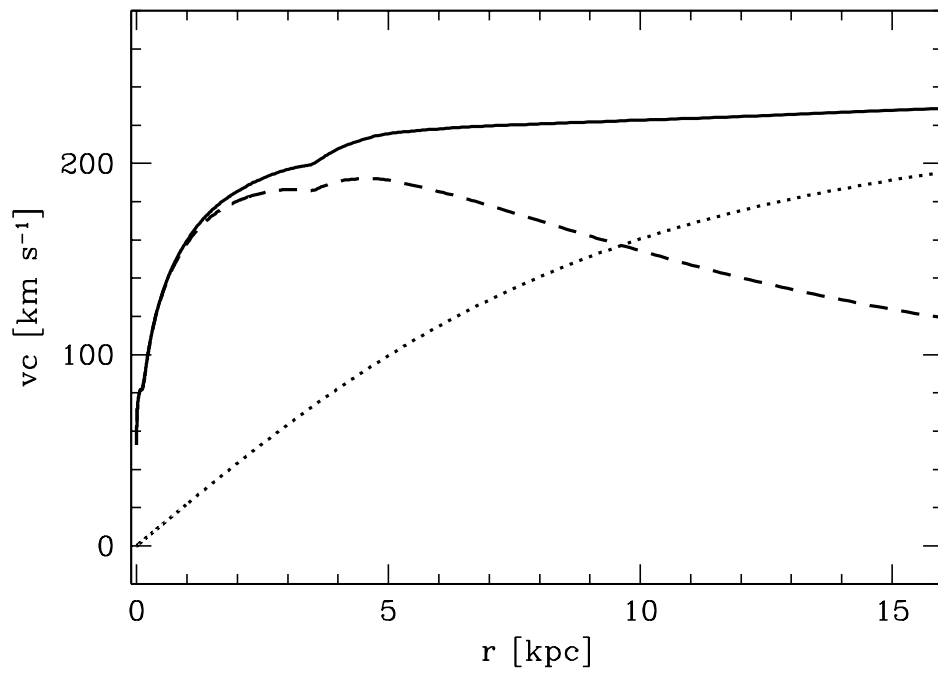


Figure 2: Rotation curve for dark matter (dotted), visible matter (dashed), and total (solid) for the model shown in Fig. 1.

when the contribution of visible matter is maximized and a constant mass-to-light ratio is assumed. Additional evidence for this result comes from microlensing statistics obtained for selected fields within the bulge. The luminous mass model is only marginally able to reach the high microlensing optical depth measurements (Bissantz *et al.* 1997; Bissantz and Gerhard 2002). Increasing the dark matter component in the model would lower the model’s predictions of the microlensing optical depth, and thus increase the discrepancies with the experimental results even more.

Turning the analysis around, we can assume that we got the contribution of the visible matter to the rotation curve right, and then calculate the rotation curve of the dark matter halo, i.e. what is left for the dark matter after subtraction of the known visible matter (see Fig. 3). The data up to R_\odot are taken from Fig. 1, and those beyond R_\odot are taken from Merrifield (1992)¹ who derived them from the HI layer thickness. Clearly, within the solar orbit, the dark matter halo contribution to the rotation curve rises approximately linearly with radius. At small radii, the data again are strongly affected by non-circular motions in the bar potential. The data seem to suggest that we start to see the turnover, and that the halo scale radius is $\sim 15 \pm 5$ kpc, but the scatter in the data points beyond R_\odot is quite large. Moreover, Binney and Dehnen (1997) criticized that the increased scatter and apparently linear rising rotation curve beyond the solar radius can be explained naturally, if tracers beyond R_\odot are concentrated in a ring at $1.6R_\odot$. If Binney and Dehnen are correct, this would imply that lower values for the halo scale radius a are also possible.

The analysis so far has assumed that the gas motions can be approximated by circular orbits. However, in the bar region ($R < 3$ kpc) this is not the case and at larger radii we may have significant perturbations due to spiral arms or orbit family changes at resonances. A more detailed analysis, however, is possible with gas dynamical models which take these factors into account.

4 Orbits and resonances

The most important orbital families in the galactic plane of a barred galaxy are the so-called x_1 - and x_2 -orbits. The former exist inside the corotation resonance (CR), where one rotation of the bar takes as long as one circular orbit period. The x_1 -orbits are shaped by the periodic forcing of the bar and are in phase and elongated with the bar. The x_2 -orbits are perpendicular to

¹after scaling to the values of R_\odot and V_\odot assumed here.

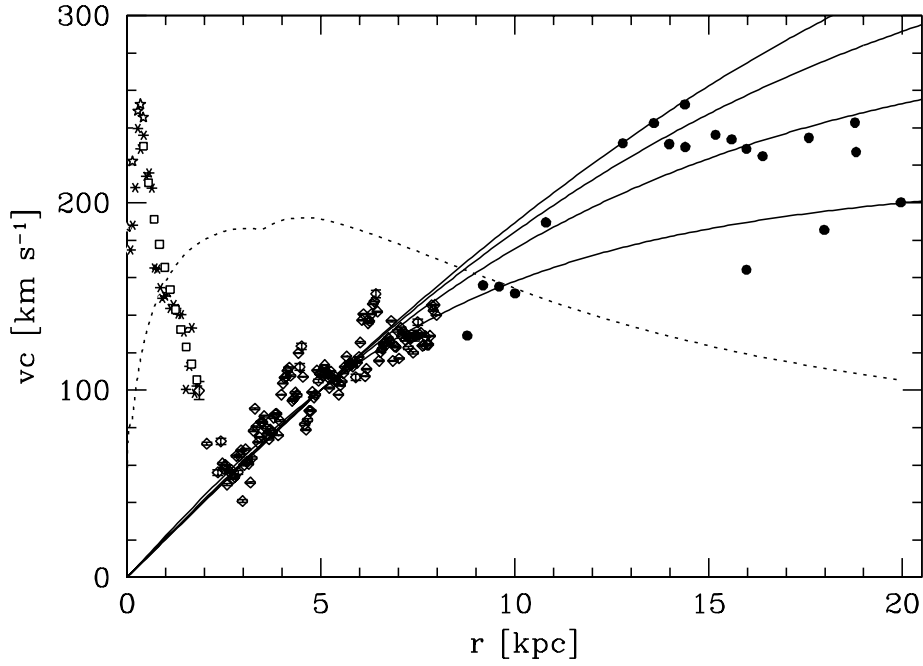


Figure 3: Dark matter halo circular rotation curve deduced from the terminal velocity curve after subtraction of the visible matter contribution (all symbols). The series of linearly rising solid curves represent isothermal dark matter halo models with parameters $(a, V) \in \{(10, 223), (15, 316), (20, 412), (25, 509)\}(\text{kpc}, \text{km s}^{-1})$ and $V/a \sim 21 \text{ km s}^{-1} \text{ kpc}^{-1}$. All these models fit the data inside $R_{\odot} = 8 \text{ kpc}$ equally well. Beyond R_{\odot} , we show data from Merrifield (1992) scaled for the values of R_{\odot} and V_{\odot} used here. This figure demonstrates that data beyond R_{\odot} is crucial for distinguishing between different halo mass models. The rotation curve for the visible matter is overlaid for comparison (dotted line).

the bar and typically almost round. They exist between the inner Lindblad resonance (ILR) and the center or between the two ILRs if present. Lindblad resonances happen when the epicycle frequency is twice the difference between the pattern speed and orbital angular speed. Inside corotation we can have typically one or two ILRs; outside corotation there is always a single outer Lindblad Resonance (OLR). Between CR and OLR, orbits are again elongated perpendicular to the bar but almost circular in shape.

The x_1 -orbits are considered main building blocks of the stellar bar, because they support the bar potential. They are also responsible for the sharp peak in the Milky Way’s terminal velocity curve (Binney *et al.* 1991).

Using the atomic hydrogen and molecular gas emission all sky surveys, which not only provide terminal velocity data for the inner galaxy, but also information about spiral arm tangents, etc., we can use hydrodynamical models to find further constraints for the mass model.

5 Modeling the gas dynamics

Given the mass model, one can find quasi steady state gas flow solutions by assuming some equation of state for the gas and solving the Euler equations. Here, the equation of state is assumed to be isothermal with a sound speed of 10 km s^{-1} ; and for the modeling we use a 2-dimensional smooth particle hydrodynamics (SPH) code. Artificial viscosity in the code is used to simulate shocks properly. The background potential is split into three components: axisymmetric, bar, and spiral arms. The bar and spiral arm components rotate with fixed pattern speeds Ω_b and Ω_s . Initially, the gas is set up as an exponential disk on circular orbits in the axisymmetric part of the potential. The non-axisymmetric forces due to bar and spiral arms are introduced slowly in the model to avoid transient features. The resulting gas flow is stationary in the rotating frame of the bar if bar and spiral pattern speeds are identical, or periodic if they differ. For a given set of model parameters, longitude-radial velocity diagrams for the gas are then computed as would be measured by an observer rotating with the LSR, from which we obtain the model terminal velocity curves.

For the case of a single pattern speed, the model is evolved until the gas flow is almost stationary² in the bar frame of reference. For the case of separate pattern speeds for the bar and spiral patterns, the time step corresponding to the gas flow closest to the observed gas flow is found

²A small evolution with time is always present because of the mass inflow towards the center.

by comparison with the observed atomic and molecular gas kinematics. Englmaier and Gerhard (1999) have shown that the terminal velocity curve can then be well understood in the context of gas on orbits typically found in barred galaxies. Their gas dynamical model in the barred Milky Way model potential fits the observed terminal velocity very well (see Fig. 4). Note, that the high peak at $l = 2^\circ$ is explained by non-circular motions in the bar potential and is matched better in models with higher numerical resolution. The whole process is iterative, because changing the position angle of the Sun with respect to the bar major axis requires recomputation of the mass model with the corresponding symmetry assumption, and recomputation of the gas flow in the modified potential.

6 The galactic bar and the spiral arms

The best near IR model of Bissantz and Gerhard (2002) has a 3-dimensional bar with axis ratios $1 : b : c$ where $b = c = 0.35 \pm 0.05$. The angle between the bar major axis and the line from the Sun to the Galactic Center is 20° , with the bar's near end at positive longitudes.

The corresponding mass distribution, however, contains no direct information about dynamical parameters such as pattern speeds. If we can assume that the Milky Way's bar and spiral patterns each rotate with a constant angular speed for at least a few rotations, and that the gas flow reaches a quasi-steady state, then a comparison of the model with the observed gas flow can yield constraints on the current values of both pattern speeds in the Milky Way.

In the gas dynamical model we observe spiral arms that cause large deviations from circular velocity within corotation and only small deviations outside corotation of the bar. In the Milky Way, there is the so-called '3-kpc-arm' which extends to 3 kpc in radius and has strongly non-circular motions. On the other hand, the so-called molecular ring material between $4 \text{ kpc} < r < 7 \text{ kpc}$ appears to be on nearly circular orbits. Thus we can place corotation between those limits; in the following we set the corotation radius to 3.5 kpc.

From observations and models of other barred galaxies it is known that the corotation radius is typically 1.2 ± 0.2 times the radius of the bar ends (Athanasoula 1992). Larger values would be possible if the bar were able to slow down (Debattista and Sellwood 2000). Our corotation derived above is consistent with the condition $R_{\text{CR}}/R_{\text{bar}} = 1.2 \pm 0.2$, however, if the bar length turns out to be underestimated, we would need to increase the coro-

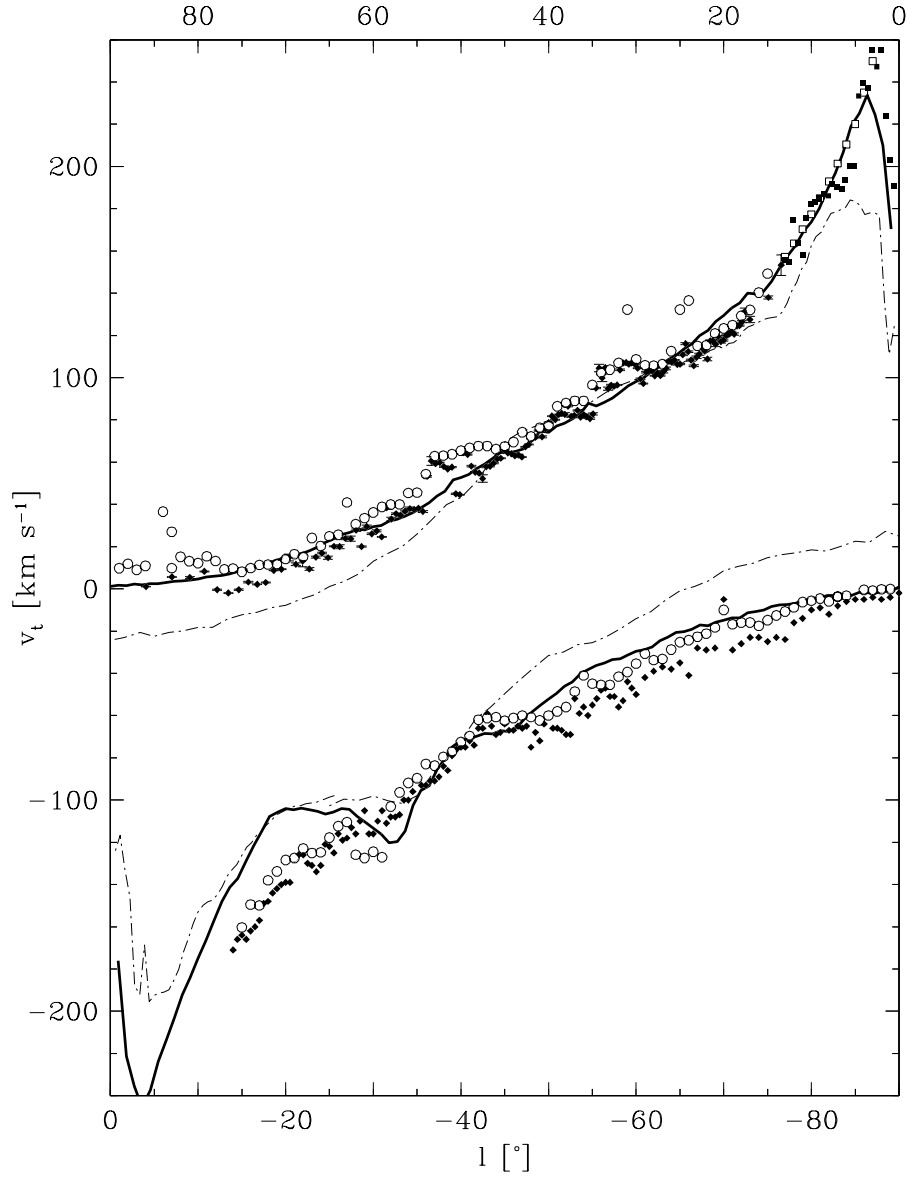


Figure 4: Gas dynamical model results for the Galactic terminal velocity curve. Data points are from various observations (see Englmaier and Gerhard (1999) for details). The upper (lower) part of the diagram shows data and models for positive (negative) galactic longitudes. The solid curve is the best model including dark matter. The dash-dotted curve is a model without dark halo.

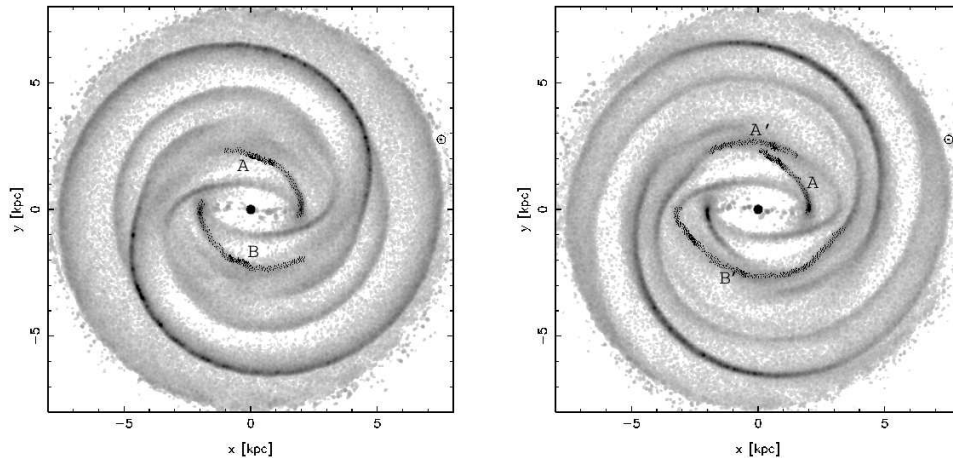


Figure 5: Gas response for models with spiral arm pattern speed set to 60 (left), and $20 \text{ km s}^{-1} \text{ kpc}^{-1}$ (right).

tation radius accordingly. Dehnen (2000) found evidence from local stellar streams that the OLR of the bar is located very close to the Sun, according to Mühlbauer and Dehnen (2003), at $\sim 0.92R_{\odot}$. If so, we can calculate the corotation radius for our model and find $R_{CR} = 4.0 \text{ kpc}$. This is in good agreement with our previous estimate.

The gas dynamical model in the barred mass model without spiral arms forms a 4-armed spiral pattern similar to the one deduced from H II-regions by Georgelin and Georgelin (1976); see Englmaier and Gerhard (1999) for the comparison. Bissantz and Gerhard (2002) used the more realistic spiral arm model of Ortiz and Lépine (1993) to improve the inversion of the inner Galaxy, and Bissantz *et al.* (2003) found the approximately periodic gas flow in this modified potential, assuming separate pattern speeds, for the bar and spiral arms.

7 Multiple Pattern Speeds

When we allow two pattern speeds in the model, i.e. the spiral pattern is given a different pattern speed from that of the bar, then the gas flow is changing in a periodic fashion with the beat frequency $\Omega_b - \Omega_s$. This periodic oscillation is strongest in the transition region between bar and spiral pattern around the bar's corotation. Because of the lower pattern speed, the spiral pattern extends to larger radii; its outer radius is approximately given by

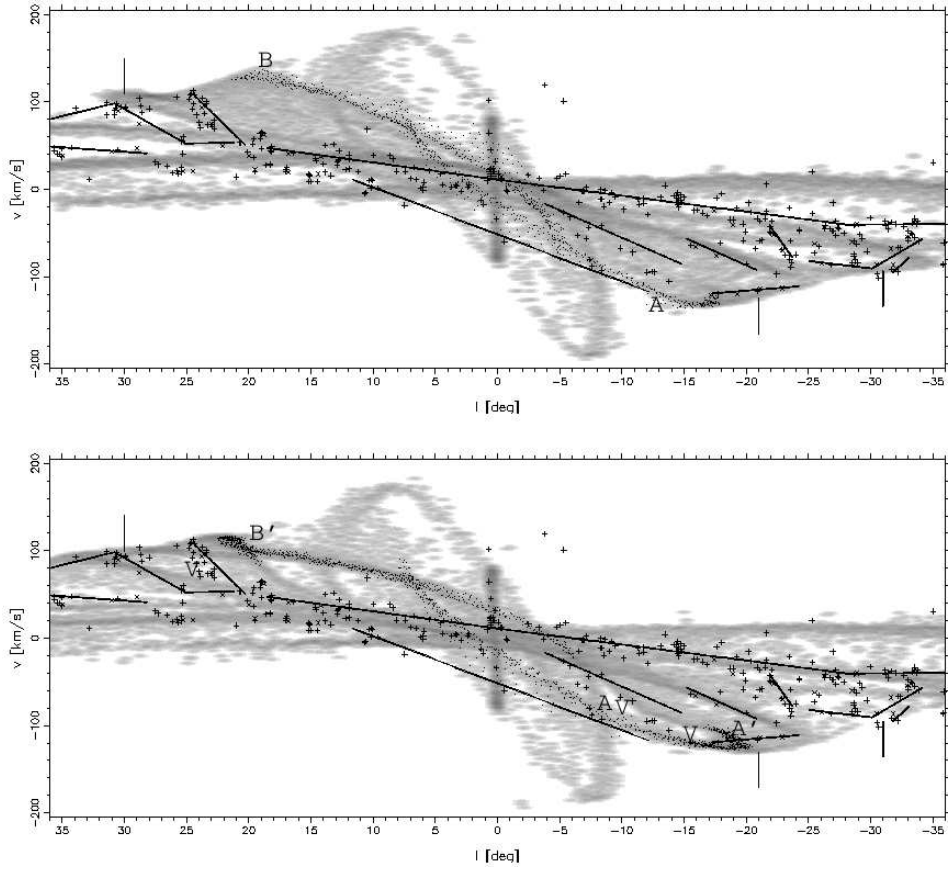


Figure 6: (l, v) diagrams for models with fast ($60 \text{ km s}^{-1} \text{ kpc}^{-1}$; top) and slow spiral arms ($20 \text{ km s}^{-1} \text{ kpc}^{-1}$; bottom) as shown in Fig. 5. Only the slow model shows low density voids (marked as 'V') similar to those known from observations.

its OLR.

Distant faint gaseous spiral arms have been found out to radii³ of 12–16 kpc (Davies 1972), and even 17–22.6 kpc (McClure-Griffiths *et al.* 2004). However, it could well be possible that the outermost spiral arms are transient and do not follow the same pattern speed. Hence, it is not practical to use the radial extent to estimate the spiral arm pattern speed.

In the model with two pattern speeds, most of the time the spiral pattern beyond bar corotation smoothly connects to the inner spiral pattern driven by the bar (Fig. 5). However, because of the different pattern speeds, the outer spiral arms regularly separate from the bar-driven inner arms around corotation. On the other hand, when spiral pattern and bar rotate with the same pattern speed, the spiral pattern weakens in the corotation region and disappears. This is consistent with density wave theory, which asserts that density waves become evanescent in the region around corotation, and decay. When two pattern speeds are used, we observe in the model that the spiral pattern passes through the bar’s corotation and through the spiral arms’ corotation radius without weakening. A detailed comparison of the model with the observed gas flow shows that certain gas poor regions in the observed longitude-radial velocity diagram correspond to inter-arm regions in the gas flow near CR which only exist in the corotation region when spiral arms and bar rotate with different pattern speeds (Fig. 6). The observed gas dynamics clearly shows such gas poor regions, hence the spiral arms must rotate more slowly than the bar (Bissantz *et al.* 2003). Approximate agreement with observations is found when a pattern speed of $20 \text{ km s}^{-1} \text{ kpc}^{-1}$ is assumed for the spiral arms.

Detailed observations by Naoz and Shaviv (2005) of the spatial separation of spiral arms and young star clusters that have moved away from their spiral arms, also indicate not only that the spiral pattern rotates much slower than the bar, but also that multiple pattern speeds are present in the spiral pattern which fall into two groups around 18 and $30 \text{ km s}^{-1} \text{ kpc}^{-1}$. This observational result is also in agreement with the theory of Lin & Shu (1964) and a general result from n-body simulations of disk galaxies, namely that spiral arms are in fact not steady-state but recurrent and multiple modes overlap each other (e.g. Fux 1999).

³Rescaled to correct for the assumed distance of 8 kpc to the Galactic Center.

8 Discussion

In this review, we gave an overview of the results obtained from reconstruction of the present state of the Milky Way using near-IR luminosity and gas kinematics complimentary data sets. From the luminosity data alone, one could not infer anything about the dark matter component. Likewise, the observed gas kinematics alone is difficult to interpret and has lead historically to wrong conclusions, such as steep drops in the inferred rotation curve, large dark matter components, and explosions in the galactic center. We avoid using parametric models for describing the important bulge region which is best described as a barred bulge. This bar in the galactic center explains the observed asymmetry in the near-IR light distribution within the bulge region as well as the high non-circular gas motion inside 3 kpc galactocentric radius.

The inferred mass density is in good agreement with micro-lensing optical depth observations which provide an important independent test. The molecular ring material, is interpreted as four tightly wound spiral arms in approximate circular rotation outside the corotation radius of the bar. Models indicate that the spiral arm pattern rotates much slower than the bar, allowing the arms to extend beyond the solar orbit. Most importantly, the model has provided evidence for the maximum disk hypothesis and the amount of dark matter present inside the solar radius. Future and presently ongoing observational surveys will provide even more detailed data which will allow us to improve the model further. The next revision of the Milky Way models will probably allow more detailed studies of the spiral arms and locate more resonances.

Acknowledgments

This work was supported by Swiss Nationalfonds grant 200020-101766.

References

- Athanassoula, E.: 1992, ‘The existence and shapes of dust lanes in galactic bars’, *MNRAS* **259**, 345–364.
- Benjamin, R.A. *et al.*: 2005, ‘First GLIMPSE Results on the Stellar Structure of the Galaxy’, *ApJ Letter*, in press.

- Binney, J., Gerhard, O.E., Stark, A.A., Bally J., Uchida, K.I.: 1991, ‘Understanding the kinematics of Galactic Centre gas’, MNRAS, **252**, 210.
- Binney, J., Dehnen, W.: 1997, ‘The outer rotation curve of the Milky Way’, MNRAS **287**, L5–L7.
- Binney, J., Gerhard, O.E.: 1996, ‘On the deprojection of the Galactic bulge.’, MNRAS, **279**, 1005–1010.
- Bissantz, N., Englmaier, P., Binney, J., Gerhard, O.: 1997, ‘The microlensing optical depth of the COBE bulge’, MNRAS **289**, 651–659.
- Bissantz, N., Gerhard, O.E.: 2002, ‘Spiral arms, bar shape and bulge microlensing in the Milky Way’, MNRAS, **330**, 591–608.
- Bissantz, N., Englmaier, P., Gerhard, O.: 2003, ‘Gas dynamics in the Milky Way: second pattern speed and large-scale morphology’, MNRAS **340**, 949–968.
- Burton, W.B., Liszt, H.S.: 1993: ‘Kinematics of neutral gas in the bulge of the Milky Way’, A&A **274**, 765–774.
- Clemens, D.P.: 1985, ‘Massachusetts-Stony Brook Galactic plane CO survey—The Galactic disk rotation curve’, A&A **295**, 422–428.
- Davies, R.D.: 1972, ‘Observations of the outer spiral structure of the Milky Way and its relation to the high velocity clouds’, MNRAS **160**, 381–406.
- Dehnen, W.: 2000, ‘The effect of the outer Lindblad resonance of the galactic bar on the local stellar velocity distribution’, ApJ **119**, 800–812.
- Debattista, V.P., Sellwood, J.A.: 2000, ‘Constraints from Dynamical Friction on the Dark Matter Content of Barred Galaxies’, ApJ **543**, 704–721.
- Dwek, E., *et al.*: 1995, ‘Morphology, near-infrared luminosity, and mass of the Galactic bulge from COBE DIRBE observations’, ApJ **445**, 716–730.
- Eisenhauer, F., Schödel, R., Genzel, R., Ott, T., Tecza, M., Abuter, R., Eckart, A., Alexander, T.: 2003, ‘A Geometric Determination of the Distance to the Galactic Center’, ApJ *Letters* **597**, 121–124.
- Englmaier, P., Gerhard, O.E.: 1999, ‘Gas dynamics and large-scale morphology of the Milky Way galaxy’, MNRAS **304**, 512–434.

- Feast, M., Whitelock, P.: 1997, ‘Galactic kinematics of Cepheids from HIP-PARCOS proper motions’, *MNRAS* **291**, 683–693.
- Fich, M., Blitz, L., Stark, A.A.: 1989, ‘The rotation curve of the Milky Way to $2 R_{\odot}$ ’, *ApJ* **342**, 272–284.
- Fux, R.: 1997, ‘3D self-consistent N-body barred models of the Milky Way. I. Stellar dynamics’, *A&A* **327**, 983–1003.
- Fux, R.: 1999, ‘3D self-consistent N-body barred models of the Milky Way. II. Gas dynamics’, *A&A* **345**, 787–812.
- Georgelin, Y.M., Georgelin, Y.P.: 1976, ‘The Spiral Structure of Our Galaxy Determined from HII Regions’, *A&A* **49**, 57–79.
- Kalirai, J.S., Fahlman, G.G., Richer, H.B., Ventura, P.: 2004, ‘The Galactic Inner Halo: Searching for White Dwarfs and Measuring the Fundamental Galactic Constant, Θ_0/R_0 ’, *ApJ* **601**, 277–288.
- Kent, S.M.: 1992: ‘Galactic structure from the SPACELAB infrared telescope. III. A dynamical model for the Milky Way bulge’, *ApJ* **387**, 181–188.
- Lin, C.C., Yuan, C., Shu, F.H.: 1969, ‘On the spiral structure of disk galaxies. III. Comparison with observations’, *ApJ* **155**, 721–746.
- McClure-Griffiths, N.M. and Dickey, J.M. and Gaensler, B.M. and Green, A.J: 2004, ‘A Distant Extended Spiral Arm in the Fourth Quadrant of the Milky Way’, *ApJ* **607**, L127–L130.
- Majewski, S.R., *et al.*: 2004, ‘Taking Measure of the Milky Way’, In: S. Unwin and S. Turyshev (ed.), ‘SIM Planet Quest, Science with the Space Interferometry Mission’, JPL Publication 2004-19, pp. 15–17.
- Merrifield, M.R.: 1992, ‘The rotation curve of the Milky Way to $2.5 R_{\odot}$ from the thickness of the H I layer’, *AJ* **103**, 1552–1563.
- Mühlbauer, G., Dehnen, W.: 2003, ‘Kinematic response of the outer stellar disk to a central bar’, *A&A* **401**, 975–984.
- Naoz, S., Shaviv, N.J.: 2005, ‘Open cluster birth analysis and multiple spiral arm sets in the Milky Way’, *ApJ*, submitted, astro-ph/0503127.
- Ortiz, R., Lépine, J.R.D.: 1993, ‘A model of the Galaxy for predicting star counts in the infrared’, *A&A* **279**, 90–106.

- Reid, M.J.: 1993, ‘The distance to the center of the Galaxy’, *ARA&A* **31**, 345–372.
- Reid, M. J., Brunthaler, A.: 2004, ‘The Proper Motion of Sagittarius A*. II. The Mass of Sagittarius A*’, *ApJ* **616**, 872–884.
- Steinmetz, M.: 2003, ‘RAVE: the RAdial Velocity Experiment’, In: U. Munari, ‘GAIA Spectroscopy: Science and Technology’, *ASP Conf. Proc.* **298**, p. 381.